Review and comparison of empirical friction coefficient formulation for multibody dynamics of lubricated slotted joints

Marco Cirelli [1]*, Matteo Autiero[1], Nicola Pio Belfiore[2], Giovanni Paoli [1], Ettore Pennestrì[1], Pier Paolo Valentini[1]

[1] Department of Enterprise Engineering
University of Rome Tor Vergata
via del Politecnico 1, 00133 Rome, Italy
marco.cirelli@uniroma2.it*
[matteo.autiero,giovanni.paoli]@uniroma2.it
pennestri@mec.uniroma2.it
valentini@ing.uniroma2.it

[2] Dept. Industrial, Electrical
and Mechanical Engineering,
University "Roma Tre"
Via della Vasca Navale 79, 00146 Rome, Italy
nicolapio.belfiore@uniroma3.it

Abstract

In recent times, many industrial applications demand innovative energy-efficient solutions. One of the main causes of energy loss is due to friction between body surfaces in contact. There is a great amount of research aimed to understand the friction mechanisms to allow its reliable prediction during multibody simulation. In the fifties and sixties of the 20th Century, many investigations carried out experimental activities that led to coefficient of friction formulas for lubricated surfaces under a combination of sliding and rolling relative motion. The formulas have been mainly deduced by mathematical fitting of results obtained with experimental measurements on rolling disks and different load, lubricating and kinematic conditions. The purpose of this paper is twofold: on the one hand, reviewing semi-empirical formulas for the computation of friction coefficient in lubricated contact under different operating conditions; on the other hand, embodying and comparing, in multibody dynamics simulation environment, contact force models coupled with the metal-metal lubricated empirical friction formulas. The implementation of empirical formulas is straightforward and computationally efficient, but one can evaluate the performance of these models in characterising the dynamics of the lubricated joint. With this purpose, multibody simulation of a scotch-yoke mechanism and a Whitworth quick return mechanism with non-ideal prismatic joint are conducted. The existence of clearance causes the dynamic behaviour of the system to be different from the ideal joint. The difference between each friction coefficient model is emphasized by the means of both simulation output and computation time.

Keywords: Contact dynamics, Lubricated joints, Joint clearance, Multibody dynamics, Friction models.

Nomenclature

α	Piezo-viscosity coefficient of the lubricant
δ	Contact penetration
$\dot{\delta}$	Contact penetration velocity
$\dot{\delta}_0$	Impact velocity
η_0	Dynamic viscosity of the lubricant
λ	Specific film thickness
μ	Friction coefficient
ν_0	kinematic viscosity of the lubricant
ω	Rotational speed
ρ	Density of the lubricant
ϑ	Rotational angle
c_d	Dynamic correction factor

c_r Restitution coefficient

E Young's modulus

f_n Normal contact force per unit length

F_n Normal contact force

F_t Friction Force

G Material parameter of the Hamrock and Dowson formulation

h_c Oil central film thickness

K Contact stiffness

L Contact width

n Stiffness exponent

R_e Equivalent radius of curvature

R_i Curvature radius of surface i

S Surface roughness

U Velocity parameter of the Hamrock and Dowson formulation

V_0 Static threshold velocity

V_1 Dynamic threshold velocity

V_Σ Sum of profiles velocities

V_e Lubricant entraining velocity

V_r Rolling velocity

V_s Sliding velocity

W Load parameter of the Hamrock and Dowson formulation

1 Introduction

The earliest documented experiments on rolling friction are due to Coulomb [1]. His experiments, verified and extended by Navier and Morin [2], have been considered for years *the laws of resistance to rolling*. Based on the observation of a roller iron rolling on india-rubber surface, Reynolds [3] confirmed the observations of Coulomb and proposed a physical explanation assuming the causes of rolling resistance to be the same as those of sliding friction. This justifies the term of *rolling-friction* he introduced. During the 1950s and 1960s of the 20th Century, several experimental studies suggested many formulations of the friction coefficient for lubricated surfaces under a mixed relative motion of sliding and rolling. The formulas have been mainly deduced by mathematical fitting of results obtained with experimental measurements on rolling disks and different load, lubricating and kinematic conditions. The idea of a disk-based experimental apparatus for investigating the friction between surfaces in lubricated line contact dates back to Merritt [4]. By means of this approach, Merritt produced a series of plots that allowed a practical and prompt estimate of friction and mechanical efficiency of gears. As a result, the Merritt's testing analogy between rolling disks and meshing gears inspired many investigators that improved and adapted to their purposes the original experimental apparatus based on disks test machines. This greatly contributed to the interpretation and understanding of many complex phenomena governing the resistance between curved surfaces under relative motion. For instance, Tabor *et al.* [5, 6, 7], Hersey [8, 9] offer an extensive historical review about experimental activities on rolling friction. Martin [10] discusses various analyses about the effects of rolling and sliding friction in gear drives. Many industrial applications demand innovative, energy-efficient solutions. Friction between bodies in contact with one other's surfaces is one of the major sources of energy loss. Thoughtful investigations have been dedicated to better understand the mechanisms of friction in order to comprehend these phenomena and provide accurate estimations. The emphasis of this study is on metal-metal lubricated joints, where a fluid film is interposed between contacting surfaces to reduce friction. Some researchers (e.g. Michlin [11], Stefanelli *et al.* [12], Flores *et al.* [13, 14], Zhao *et al.* [15, 16, 17]) investigated the multibody dynamics modeling of lubricated joints. Within multibody dynamics simulations, empirically based formulas offer a concise and computationally efficient engineering approach to simulate complex friction phenomena in metal-metal lubricated slotted joints. These formulas have often been adopted in gear dynamics simulation (e.g. [18, 19]). In recent years, Peng *et al.* focused to identify novel approaches to compute friction force in complex scenarios [20, 21], in particular regarding sliding cables[22, 23].

However, a survey on the application of the friction coefficient formulas in multibody dynamics simulation does not seem to be available. With the focus on the multibody dynamics simulation of a scotch-yoke linkage with a straight slot, the purpose of this paper is twofold:

- to review semi empirical formulas and provide a compiled list of friction coefficient formulations deduced mainly by fitting of experimental data;
- to embody and compare, in multibody dynamics simulation environment, contact force models (e.g. [24, 25, 26]) coupled with the metal-metal lubricated empirical friction formulas and evaluate the possibility of employing these formulations bypassing the solution of the elasto-hydrodynamic problem (e.g. Reynolds equation).

In summary, this research enhances understanding of the distinctions among the different models and could provide guidelines for selecting the suitable friction formulation, contingent upon the specific application requirements.

2 Contact force models

The elastic contact force models play an important role in multibody dynamics simulation of mechanical systems with clearances in the kinematic pairs. Many investigations and reviews have been dedicated to the topic (e.g. [25, 26, 27, 28, 29, 30, 31]) and it is out of the scope of this work to analyse the plethora of formulation available in literature. One of the most extensively used formulation for contact force is the one proposed by Lankarani and Nikravesh [32]. The kinetic energy lost as a result of internal damping allows to estimate the hysteresis-damping factor. The loss of kinetic energy is evaluated based on the kinetic energy prior to and following the contact (*i.e.* restitution coefficient c_r) as well as the normal component of the relative contact velocity at the beginning of the contact-impact event $\dot{\delta}_0$. In particular, the normal contact force is evaluated as

$$F_n = K\delta^n \left(1 + \frac{3}{4}\frac{\dot{\delta}}{\dot{\delta}_0}(1 - c_r^2)\right) \tag{1}$$

where K is the contact-stiffness parameter, δ represents the relative penetration between bodies in contact, and n is the exponent representing the non-linear relation between penetration and force depending on the material and the local geometrical properties of contacting bodies. This model was developed for the case of two spheres in contact; however, it is also used for cylindrical contact by adjusting the contact stiffness K and the exponent n [33]. To evaluate these parameters, the Johnson model [34] was used, which, however, requires an iterative solution due to the implicit nature of the equation. In order to overcome this shortcomings, Autiero *et al.* [26] expressed the force penetration relations with parametric fitted polynomial of the type

$$F_n = K\delta^n \tag{2}$$

in order to speed up the computation with relatively low error. To this extent, in Figure 1, the correlation between the contact force per unit length f_n and the penetration δ is reported using the Johnson model for various values of the clearance c for both steel (left) and aluminum (right).

A dry frictionless contact produces only a force that is normal to the surfaces in contact; conversely, friction simultaneously generates a tangential component. Contact force models for cylinders are employed in the evaluation of normal component, while for the friction force some precautions are needed to avoid numerical difficulties. Among the plethora of possibility for the evaluation of friction force preventing numerical problems in dry [35] and lubricated [36] contacts, only the one chosen for the application in Section

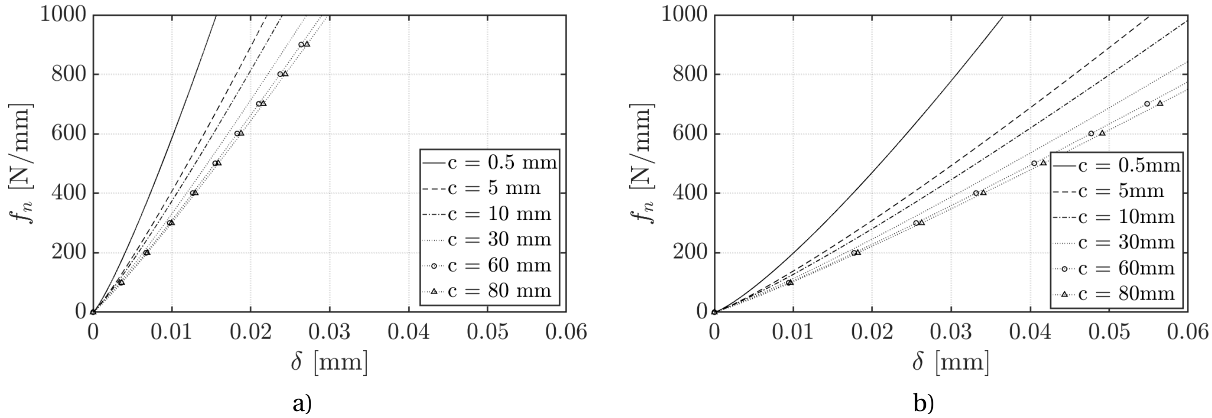

Figure 1: Plots of the cylindrical Johnson contact-force model [34]. a) Steel, b) Aluminum.

5 is briefly discussed. The friction model, reported in [14], consists in a modified Coulomb force expressed as

$$F_T = -c_d \mu F_n \frac{\vec{V}_s}{|\vec{V}_s|} \tag{3}$$

where μ represents the friction coefficient and the dynamic correction factor c_d prevents the friction force from changing direction for negligible tangential velocity values, minimizing numerical issues. This factor is defined as

$$c_d = \begin{cases} 0 & \text{if} \quad |\vec{V}_s| \leq V_0 \\ \frac{|\vec{V}_s| - V_0}{V_1 - V_0} & \text{if} \quad V_0 \leq |\vec{V}_s| \leq V_1 \\ 1 & \text{if} \quad |\vec{V}_s| \geq V_1 \end{cases} \tag{4}$$

in which V_0 and V_1 are the threshold velocities for the sliding speed. It is important to underline that this friction model does not take into account stiction, but only sliding.

In this paper, the normal contact force and the friction model described in Equation 1 and 3 are embedded in multibody dynamic simulations that involve dry contact phenomena and mixed lubrication conditions. In the former case, we consider both absence of friction and presence with a constant friction coefficient $\mu = 0.1$. In the latter case, friction coefficients that vary instantaneously depending on operational conditions, as described in Section 3, are employed. From a strict perspective, the lubricant impacts the normal force by affecting the contact stiffness. In particular, the overall stiffness of the normal contact force should be computed as a series of springs: once due to the lubricant, the other one due to the contact surfaces.However, in mixed lubrication conditions, the most significant contribution to the system's stiffness is due to the deformation of the surfaces. At the same time, the oil film contributes minimally to the stiffness of the system itself [37]. Under this hypothesis, it is possible to neglect the stiffness contribution of the lubricant on the contact stiffness. According to [37], the main effect of the lubricant is damping the system. However, this paper does not intend to focus on the influence that the lubricating film has on the damping of the system; therefore, as a first approximation, the authors consider it reliable to use the dry contact formulation in partial elasto-hydrodynamic lubrication.

3 Review of friction coefficient formulations

Many researchers conducted experimental work in the fifties and sixties of the 20th century that led to coefficient of friction formulas for lubricated surfaces under a combination of relative sliding and rolling motion [7]. The formulas were mainly derived by mathematical fitting of results obtained from experimental measurements of rolling disks under different loads, lubricants and kinematic conditions. Most sliding contacts are lubricated, in this case friction decreases with increasing sliding speed up to the formation of a sufficiently thick lubricant film. After that, a mixed or full film condition is observed and the friction coefficient can either be constant, raise or decrease with increased sliding speed [36]. This phenomenon was described by Stribeck [38], whose name is often associated with sliding friction in lubricated contacts running under boundary, mixed, and full film conditions. The lubrication regime and its effect on friction is depicted in Figure 2, where the so-called Stribeck curve is qualitatively illustrated. In boundary lubrication (region A), the load is mostly carried by asperities and the lubricant acts at monomolecular scale [39]. Hence, the type of the lubricant and the mating surfaces are the primary factor of boundary friction, which is relatively unaffected by speed, load, and lubricant viscosity. At low loads and relatively high speed, hydrodynamic lubrication regime is reached (region C). A thick layer of lubricant now completely separates the surfaces and the friction is calculated from Reynolds equations. The region B is called mixed lubrication where the load is shared among fluid and asperities. Despite a few exceptions, mixed lubrication region is where the majority of gear applications are found. Low speed gears that are severely loaded exhibit symptoms of being in the boundary region, while lightly loaded high speed gears may achieve complete fluid film lubrication. All friction coefficient models, obtained for gear application, are evaluated for mixed lubrication conditions, which means that in quantitative terms the specific film thickness (*i.e.* $\lambda = h_c/S$, with h_c and S the central film thickness and composite surface roughness, respectively) assume values between 0.5 and 3 [40].

The authors of this paper are well aware that more sophisticated models have been developed for mixed lubrication condition and available in the current technical literature, especially regarding the definition of the friction coefficient for two mating gears [41, 42] and these are crucial to have results in agreement with experimental data [43]. However, the present investigation focuses on simplified models that could be conveniently embedded in the algorithms for the dynamic simulations of multibody systems working under non stationary conditions, with the intent of establishing a trade-off between computational efficiency and accuracy. Moreover, the formulas herein reviewed have been also embodied in gear dynamics modelling and experimentally validated [10, 44, 18]. In Table 1, the reviewed friction coefficient formulations are displayed reporting units and application bound where available. Referring to the table, μ represents the friction coefficient, ν_0 the kinematic viscosity at mean surface temperature, η_0 the dynamic viscosity at

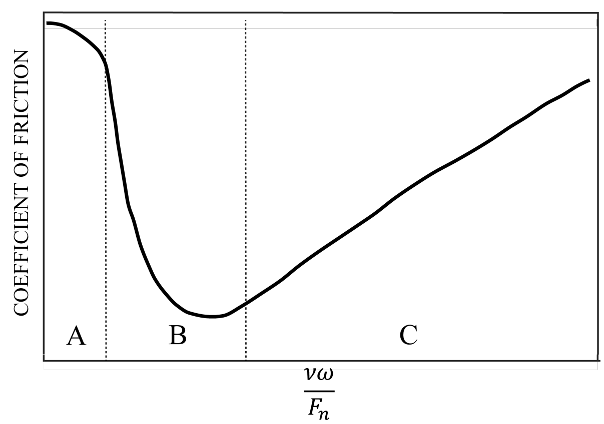

Figure 2: Stribeck curve: friction coefficient varying the ratio between the product viscosity times rotational speed ($\nu\omega$) and the load F_n.

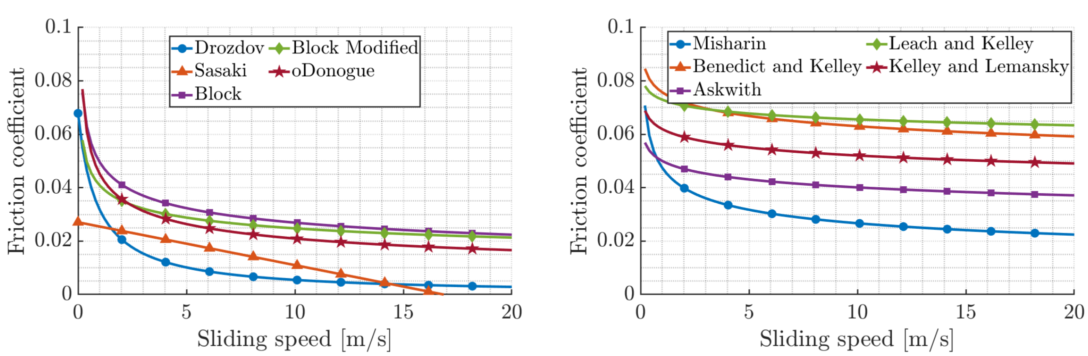

Figure 3: Friction coefficient varying sliding speed with constant load (F_n = 2000 N) for different semi-empirical formulations.

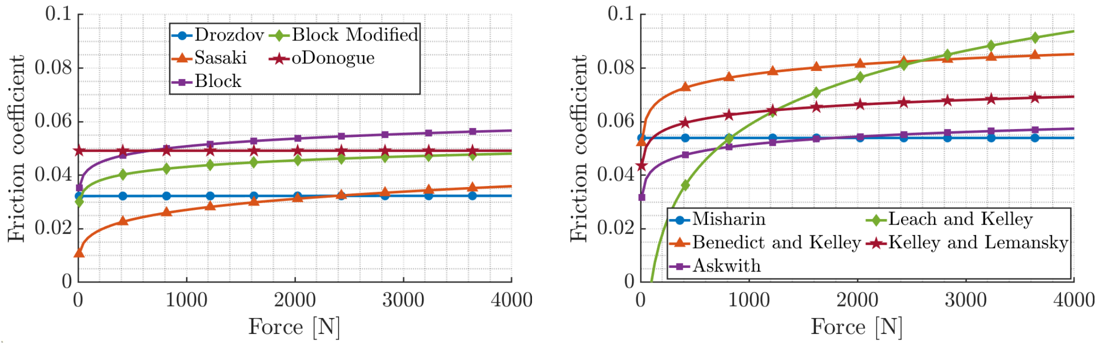

Figure 4: Friction coefficient varying load with constant sliding speed (V_s = 1 m/s) for different semi-empirical formulations.

mean surface temperature, f_n the normal load per unit length, V_s the sliding speed, V_Σ the sum of profiles velocities, V_r the rolling speed (*i.e.* $V_r = V_\Sigma/2$), S the surface roughness and R_e the effective radius of curvature (*i.e.* $R_e = R_i R_j/(R_i + R_j)$, where R_i and R_j are respectively the radius of curvature of profile i and j). If there is no direct indication on the formula applicability range, one can refer to single articles and take the experiments conditions in terms of viscosity velocities and load as reference. Moreover, in Table 2, measurement units of presented formulas are reported while in Table 3 parameters adopted for friction coefficients comparison are summarized.

Even though all the researchers provided different formulation for the friction coefficient, their observations in mixed condition (*i.e.* region B in the Stribeck curve) are quite similar and summarized below:

- the entraining lubricating fluid kinematic viscosity (ν_0) has a strong effect on the friction coefficient. They observed a rise in friction coefficient with reduced ν_0 apart from cases where there were small sliding speed and high rolling speed (*i.e.* surface speed sum V_Σ). The bigger the sliding speed the higher the effect of viscosity on friction coefficient;

- the friction coefficient lowers when rolling velocity V_Σ increases. This effect is more significant with reduced load, viscosity and sliding speed. The same behaviour can be observed for the sliding speed V_s;

- increasing the load f_n (*i.e.* the contact pressure) results in an higher friction coefficient.

Due to the complexity of the physical phenomenon we are dealing with, the formulas seem to yield a friction coefficient that is not dimensionless. This issue has been solved through the proportionality coefficients present in all formulations. Furthermore, it is important to note that these friction coefficients are derived from fitting experimental data, thus incorporating dynamic effects related to friction phenomena such as pre-sliding displacement, Dahl effect, and frictional lag. Therefore, by using these coefficients within the static friction model described in Equation 3, the overall internal dynamics of friction are taken into account collectively.

Due to the experimental observation agreement in this regime of lubrication, the empirical formulas reported are similar from the physical quantity dependence viewpoint. In addition to all the physical quantities mentioned above that influence the friction coefficient, Kelley & Lemanski propose, without experimental evidence, a factor dependent on gear dimensions by the means of the radii of curvature. O'Donaghue & Cameron are the only authors among the ones herein reviewed that directly include the surface roughness effect in the friction coefficient formulation. The other investigators either do not discuss it or give corrective coefficients. Figure 3 and 4 report comparative results of the friction coefficient computed through all different friction models as a function of the sliding speed with constant load and as a function of load with a constant sliding speed. It is noticeable how most formulations exhibit similar trends in the friction coefficient with sliding velocity, except for Sasaki and Drozdov, which show a significantly lower friction coefficient at high sliding velocities. With increasing load, however, the Leach and Kelley model shows a much more pronounced increase in the friction coefficient compared to other formulations. On the other hand, the models developed by O'Donogue, Drozdov, and Misharin show no dependence on the applied force.

Table 1: Friction coefficients under combined rolling and sliding.

Author	Formula
Y.A. Misharin[1][45, 46]	$\mu = 0.325\,(\nu_0 V_\Sigma V_s)^{-0.25}$
Sasaki[2] *et al.* [47]	$\mu = 0.758k\left(\dfrac{\eta V_r^4}{f_n^{1.7}}\right)^{-0.12}$
H. Blok[3][45]	$\mu = 0.0731\left(\eta_0 V_\Sigma^{0.85} V_s^{1.44} f_n^{-0.43}\right)^{-0.184}$
H. Blok[3][45]	$\mu = 0.0688\left(\beta_0^{-0.16}\eta_0 V_\Sigma^{1.19}\ V_s^{1.22} f_n^{-0.44}\right)^{-0.178}$
Askwith *et al.* [48, 49]	$\mu = 0.0099\log_{10}\left(\dfrac{5.642\cdot 10^3 f_n}{\eta_0 V_s V_\Sigma^2}\right)$
Benedict & Kelley [39]	$\mu = 0.0127\log_{10}\left(\dfrac{4.597\cdot 10^4 f_n}{\eta_0 V_s V_\Sigma^2}\right)$
Leach & Kelley [50]	$\mu = -0.00738\log_{10}\left[6.415\cdot 10^{48}\left(\dfrac{V_s V_\Sigma^2}{\eta_0^7 f_n^{7.9}}\right)\right]$
Kelley & Lemanski [49]	$\mu = 0.0099\log_{10}\left(\dfrac{1.618 f_n}{\eta_0 V_s V_\Sigma^2\left[\left(R_i + R_j\right)/3\right]^2}\right)$
O'Donoghue & Cameron [51]	$\mu = \left(\dfrac{39.37S + 22}{35}\right)\dfrac{0.0152}{\eta_0^{\frac{1}{8}} V_s^{\frac{1}{3}} V_\Sigma^{\frac{1}{6}} R_e^{\frac{1}{2}}}$
Drozdov & Gavrikov [4][52]	$\mu = \dfrac{1}{0.8\nu_0^{\frac{1}{2}} V_s + V_\Sigma\phi + 13.4}$

[1] Validity range $0.02 \le \mu \le 0.08$.

[2] $V_r = \dfrac{V_\Sigma}{2}$, $V_x = \dfrac{V_s}{V_r}$,

$$k = \begin{cases} 0.037 \text{ if } V_x = 0.31, \\ 0.026 \text{ if } V_x = 1.22 \end{cases} .$$

[3] $\beta_0 = 0.012\eta_0^{0.33}$ [°C^{-1}].

[4] $\phi = 0.47 - 0.13\cdot 10^{-4} p_{\max} - 0.4\cdot 10^{-3}\nu_0$, with $p_{\max}$, maximum contact pressure. $V_s \le 15$ m/s, $3 \le V_\Sigma \le 20$ m/s, $4 \le \nu_0 \le 500$ cSt, $4000 \le p_{\max} \le 20000$ kgf/cm^2.

UOM of reported formulas							
ν_0	η_0	V_s	V_Σ	f_n	p_{max}	S	R
[cSt]	[cP]	[m/s]	[m/s]	[N/m]	[kgf/cm^2]	[μm]	[m]

Table 2: Units of measure of reported formulas

ΔR [mm]	1	V_s [m/s]	[0-5]
R_1 [mm]	10	W [N]	[0-4000]
R_2 [mm]	9	E [GPa]	210
L [mm]	10	ν	0.3
S [μm]	1.6	η_{oil} [cP]	400
V_Σ [m/s]	5	ρ_{oil} [kg/m^3]	910

Table 3: Parameters for friction coefficients comparison.

4 Multibody model for comparison

4.1 Case study 1: Scotch-Yoke Mechanism

As first case study, a scotch-yoke mechanism with a straight slot, as depicted in Figure 5, has been chosen for testing different friction coefficient formulations. This mechanism is made up of four rigid bodies (crank, pin, slider and frame), two revolute joints, one prismatic joint and a non ideal joint with friction between pin and slider slot. The pin revolute joint is modelled with friction in order to avoid uncontrolled rotational speed of the pin itself, while all the other kinematic pairs are ideal and frictionless. In particular, a simplified model for the calculation of the friction torque of the pin revolute joint is considered, namely $T_p = \mu F_p R_{pi}$, where F_p is the reaction force of the kinematic pair calculated from the simulation, $R_{pi} = R_p/2$ is the inner radius of the pin and $\mu = 0.1$ is the friction coefficient. The geometrical data and inertia parameters are summarized in Table 4, while all the other parameters are listed in Table 5. For the examples herein considered, a

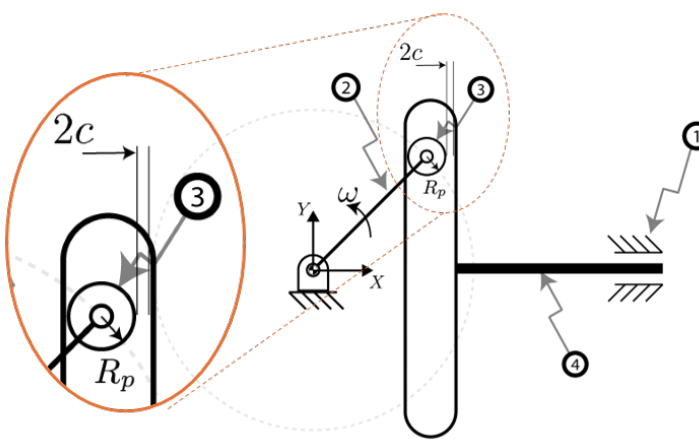

Figure 5: Scotch-Yoke mechanism with pin-slot non-ideal joint.

threshold velocity $V_0 = 0$ is chosen. This represents a limit case for the friction model reported in Equation 3 and 4. Since the sliding velocities computed during the simulations consistently exceed this chosen threshold, we are confident that different choices of the threshold do not significantly affect the overall numerical results. It is worth noting that the system taken as a case study has lubricated contacts with backlash and can not be reduced to a stationary system. It is possible to formulate the equations of motion for a dynamic system under holonomic constraints as a system of Differential Algebraic Equations (DAE). Indicated by $\boldsymbol{q}$ the vector of generalized coordinates (position and attitude) of all bodies the system can be expressed as:

$$\begin{bmatrix} \boldsymbol{M} & \boldsymbol{\Psi}_{\boldsymbol{q}}^{\boldsymbol{T}} \\ \boldsymbol{\Psi}_{\boldsymbol{q}} & \boldsymbol{0} \end{bmatrix} \begin{Bmatrix} \ddot{\boldsymbol{q}} \\ \boldsymbol{\lambda} \end{Bmatrix} = \begin{Bmatrix} \boldsymbol{Q} \\ \boldsymbol{\gamma} \end{Bmatrix} \tag{5}$$

where $\boldsymbol{M}$ is the system mass matrix, $\boldsymbol{\Psi_q}$ is the Jacobian matrix related to kinematic constraints, $\ddot{\boldsymbol{q}}$ is the vector containing generalized accelerations, $\boldsymbol{\lambda}$ is the vector of Lagrange multiplier, $\boldsymbol{Q}$ is the vector of generalized forces and $\boldsymbol{\gamma}$ can be expressed as

$$\boldsymbol{\gamma} = -(\boldsymbol{\Psi_q}\dot{\boldsymbol{q}})_q\dot{\boldsymbol{q}} - 2\boldsymbol{\Psi_{qt}}\dot{\boldsymbol{q}} - \boldsymbol{\Psi_{tt}} \tag{6}$$

From a numerical prospective, the multibody dynamic simulation is performed using the Baumgarte method [53] to ensure the stabilization of kinematic constraint violation. The contribution of contact pairs is taken into account in the force vector $\boldsymbol{Q}$ rather than in the jacobian $\boldsymbol{\Psi}$ as the kinematic joints. The acceleration vector $\ddot{\boldsymbol{q}}$ and Lagrange multipliers $\boldsymbol{\lambda}$ are computed given the initial conditions for position and velocity. The resulting acceleration is integrated to obtain velocity and position at the next time step. The numerical integration is performed using the Matlab routine *ode45*, based on the explicit Runge-Kutta method. As it is already pointed out, the cylindrical contact force models available in literature are mostly implicit. In order to speed up the computation, using the approach employed in [26], the stiffness parameter K is derived from polynomial fitting while the dissipation component is evaluated according to the Equation 1.

Geometry		Member	Mass	Inertia
Crank length	50 mm	Crank	0.300 kg	3.8e2 kg·mm^2
Slot width	16 mm	Pin	0.025 kg	7.8e-1 kg·mm^2
Slot thickness	16 mm	Slider	0.300 kg	
Clearance	50 μm			

Table 4: Geometric and inertia parameters of the Scotch-Yoke mechanism.

Young's modulus	210 GPa	Baumgarte coefficients $[\alpha, \beta]$	[5,5]
Poisson ratio	0.3	Integration step size	variable
Restitution coefficient	0.9	Integration tolerance	1e-6
Dynamic viscosity	400 cP	Crank angular velocity ω	5000 rpm
Contact stiffness K	3.42e11 N/m	Threshold velocity V_0	0 mm/s
Stiffness exponent n	1.34	Threshold velocity V_1	10 mm/s

Table 5: Data for dynamic simulation of the Scotch-Yoke mechanism.

Regarding the evaluation of contact parameters before the contact occurs, the Matlab event function is used. When a contact condition is detected, the integrator stops and the contact initialization parameters are reset (mainly the penetration speed between the surfaces, on which the damping coefficient depends). Once this is done, the code returns to the integrator and starts the calculation of the dynamics of the system. The same thing happens when the surfaces detach.

4.2 Case Study 2: Whitworth Quick return mechanism

As a second case study, a multibody model was developed for the Whitworth Quick Return Mechanism, shown in Figure 6. The mechanism consists of six bodies: frame (1), crank (2), pin (3), slotted bar (4), connecting rod (5), and slider (6). Its function is to convert the rotary motion of the crank into the translational motion of the slider; the return time of the latter is governed by the center distance l_0, the length of the crank and the offset of the slider l_1. In this case, the prismatic joint connecting the crank and the oscillating slotted bar is considered non-ideal. The same considerations regarding the friction of the pin revolute joint and the integration of contact forces within Equation 5, as applied to the Scotch-yoke mechanism, have been taken into account for this mechanism as well.

The geometric data are reported in Table 6, while the dynamic simulation parameters are presented in Table 7.

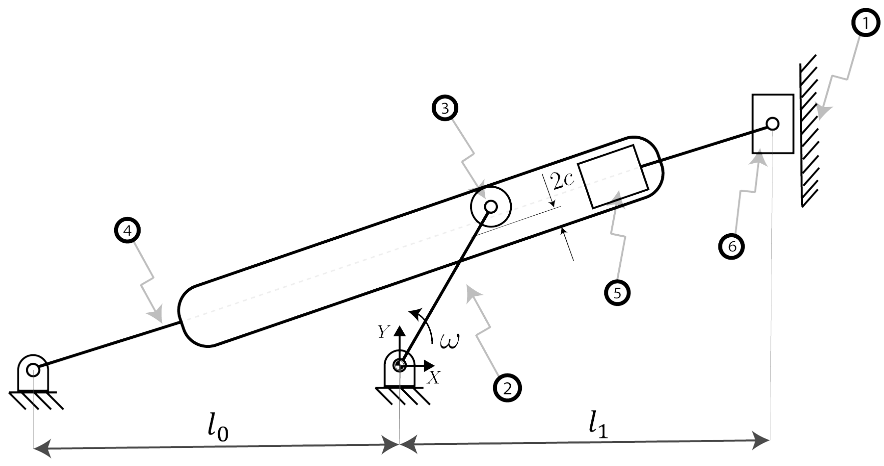

Figure 6: Whitworth quick return mechanism with pin-slot non-ideal joint.

Geometry		Member	Mass	Inertia
Crank length	80 mm	Crank	3.900 kg	1.25e4 kg·mm^2
Center distance l_0	200 mm	Pin	0.042 kg	8.00e-1 kg·mm^2
Slider offset l_1	200 mm	Slotted Bar	1.136 kg	7.35e3 kg·mm^2
Slot width	30 m	Connecting Rod	0.064 kg	9.23e-1 kg·mm^2
Slot thickness	20 mm	Slider	0.250 kg	
Clearance	20 μm			

Table 6: Geometric and inertia parameters of the Whitworth quick return mechanism.

Young's modulus	210 GPa	Baumgarte coefficients $[\alpha, \beta]$	[5,5]
Poisson ratio	0.3	Integration step size	variable
Restitution coefficient	0.9	Integration tolerance	1e-6
Dynamic viscosity	400 cP	Crank angular velocity ω	1000 rpm
Contact stiffness K	3.90e11 N/m	Threshold velocity V_0	0 mm/s
Stiffness exponent n	1.51	Threshold velocity V_1	10 mm/s

Table 7: Data for dynamic simulation of the Whitworth quick return mechanism.

5 Results and discussion

5.1 Case study 1: Scotch-Yoke Mechanism

The outcomes of three non-ideal joint with clearance cases will be shown in this section: dry without friction, dry with constant friction ($\mu = 0.1$), and lubricated joint with friction estimated by the means of previously reviewed semi-empirical models. Generally, reaction force in joint with clearance exhibits peaks not observed in the ideal joint. These spikes are generated from impact and this can result in a chaotic and non-deterministic behaviour. However, in this particular case it can be observed a periodic trend in which the solution is not affected by initial conditions. For this reason, only results for one crank full rotation are presented.

Firstly, a sensitivity analysis is conducted for the dry condition in order to highlight the effect on the interaction force of both the restitution coefficient c_r and the clearance c between pin and slot. The effect of clearance, as shown in Figure 7, is twofold. On the one hand, a larger clearance increases the impact speed by increasing the free flight time and reducing the damping effect due to hysteresis. On the other hand, the motion will be much more irregular with continuous bouncing. As a consequence, with the clearance rise, the normal force shows higher peaks and the detachment between the surfaces happens more frequently, as shown on the left side of Figure 7. Furthermore, on the right side, the trajectory of the pin center in the slider reference system is plotted. To compare the different cases as the clearance varies, the relative X coordinate has been normalized. Instead, the restitution coefficient, as it is possible to observe from Figure 8, slightly effects the oscillation frequency while has a strong influence on the oscillation amplitude. In this particular configuration, the normal force, illustrated in Figure 9, is not influenced by the friction force. This is due to the fact that normal and tangential force always lies on the same direction (either positive or negative) for each time step.

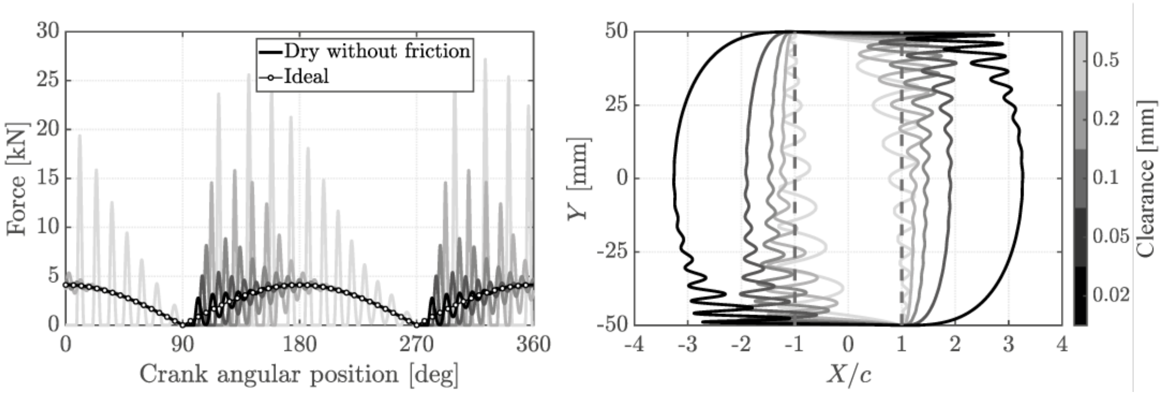

Figure 7: Clearance c sensitivity: normal contact force (left); pin center trajectory (right).

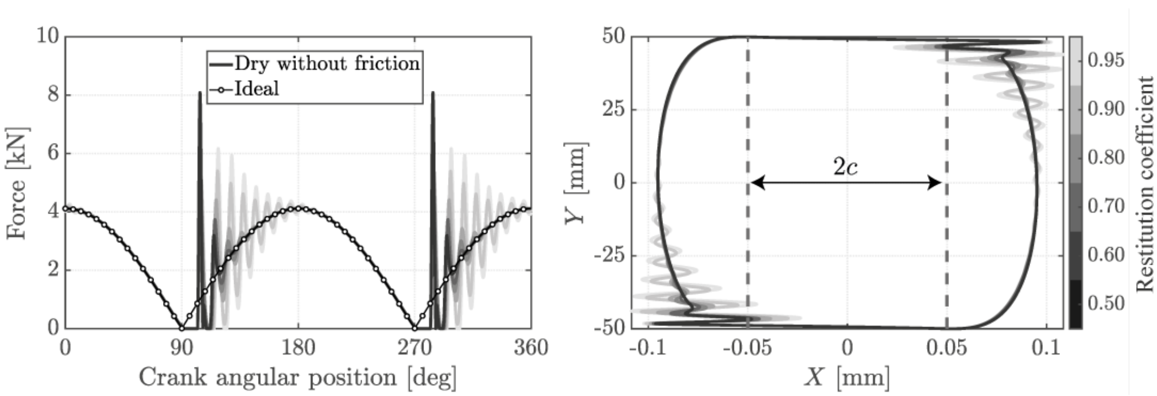

Figure 8: Restitution coefficient c_r sensitivity: normal contact force (left); pin center trajectory (right).

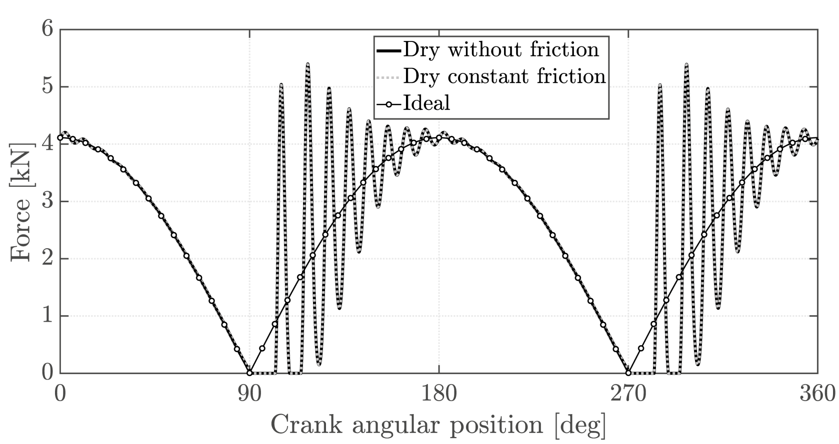

Figure 9: Comparison of normal contact force in non-ideal joint with reaction force of ideal joint.

Before the comparison of friction coefficients formulations, it is necessary to ensure that, for most of the time, the lubrication regime is mixed. As it is already been said before, the mixed condition is present when the specific film thickness λ is between 0.5 and 3. Referring to the Table 5.1 for the surface and oil parameters, it is necessary to evaluate the central film thickness throughout the simulation. To this extent, the Hamrock and Dowson formulation [54] for cylindrical contact is used. In their formulation the central film thickness h_c is

$$\frac{h_c}{R_e} = 2.69 \cdot G^{0.53} \cdot U^{0.67} \cdot W^{-0.067} \tag{7}$$

where R_e is the equivalent radius of curvature of the contacting surfaces, while G, U and W represent the material parameter, the velocity parameter and the load parameter respectively. These non-dimensional groups are defined as

$$G = \alpha E_r \tag{8a}$$

$$U = \frac{\eta_{oil} V_e}{E_r R_e} \tag{8b}$$

$$W = \frac{F_n}{E_r R_e L} \tag{8c}$$

where α is the piezo-viscosity coefficient of the lubricant, E_r is the equivalent Youngs modulus of the surfaces, η_{oil} the dynamic viscosity of the lubricant, V_e the lubricant entraining velocity (*i.e.* the average speed of the surfaces) and L is the contact thickness.

Oil properties @ 40 °C	
Type	Naphtenic
Dynamic viscosity η [cP]	400
Density ρ [kg/m^3]	910
Piezoviscosity coefficient α [GPa^{-1}]	23.4
Surface and material properties	
Composite surface roughness S [μm]	0.5
Young's modulus E [GPa]	210
Poisson ratio ν	0.3
Equivalent radius of curvature R_e [mm]	8
Pin and slider width L [mm]	16

Table 8: Oil, surface and material properties used in the simulation.

Evaluating the film thickness along one crank rotation brings to the results displayed in Figure 10. It is possible to observe that, during the motion inversions happening at $\vartheta_{crank} = \frac{\pi}{2} + k\pi$ with $k = 1, 2, ..., n$, the speed and the load are too low that the value of film thickness is undetermined. Averaging the central film thickness along one crank rotation it is found that $\overline{h_c} = 0.83\mu$m. This leads to a value of the mean specific film thickness $\overline{\lambda}$ of 1.66, which fulfils the mixed lubrication condition. It has to be highlighted that the parameter λ is strictly dependent on the operating conditions and on the lubricant, material and suface parameters. Thus, when the lubricant, surface finish, material of the bodies in contact, or operating conditions changes, this check must be carried out in order to apply these friction coefficient formulations.

Having said that, different friction coefficient models have been tested and their value are plotted versus the crank angle (Figure 11-12). Even though the different friction formulations provide similar trend, their magnitude are quite different between one and other. In particular, Misharin and Drozdov models produce extremely low values of friction coefficient during high sliding speed phases and give feasible values only when the sliding speed lowers. Furthermore, it should be noted that only the Leach and Kelley model has a distinctive trend. This fact can be explained with the strong load dependence that these authors propose in their empirical formulation causing the friction coefficient to assume the normal force trend instead of showing a predominant sliding speed effect.

Referring to the Figure 13, the trend of the driving torque is displayed in three cases: ideal case, non-ideal kinematic joint without friction, and with friction using Benedict & Kelley model. In the non-ideal joint case, the torque exhibits a dynamic behavior due to impacts that occur on the contact surfaces. Such events

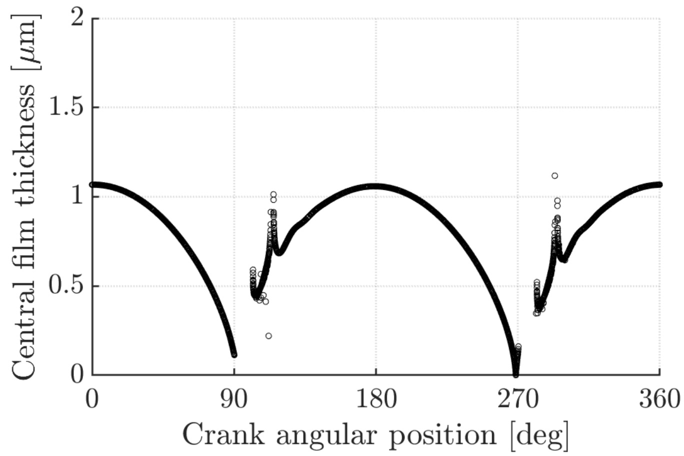

Figure 10: Central film thickness along one crank rotation.

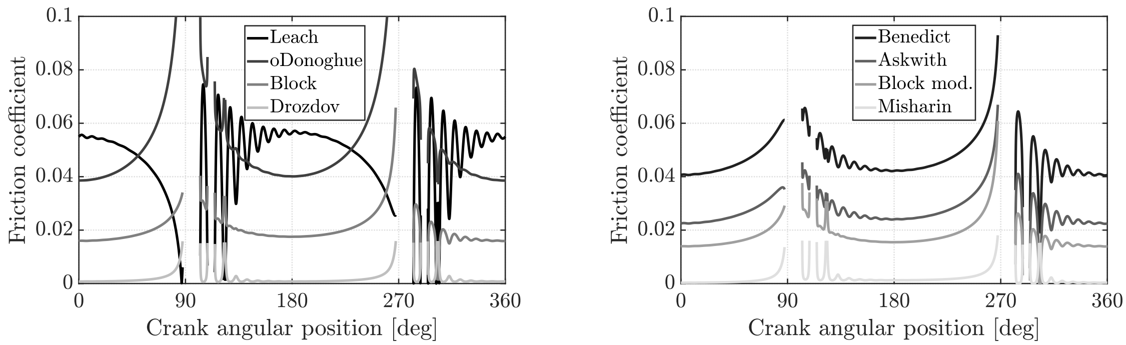

Figure 11: Friction coefficient for different semi-empirical formulations.

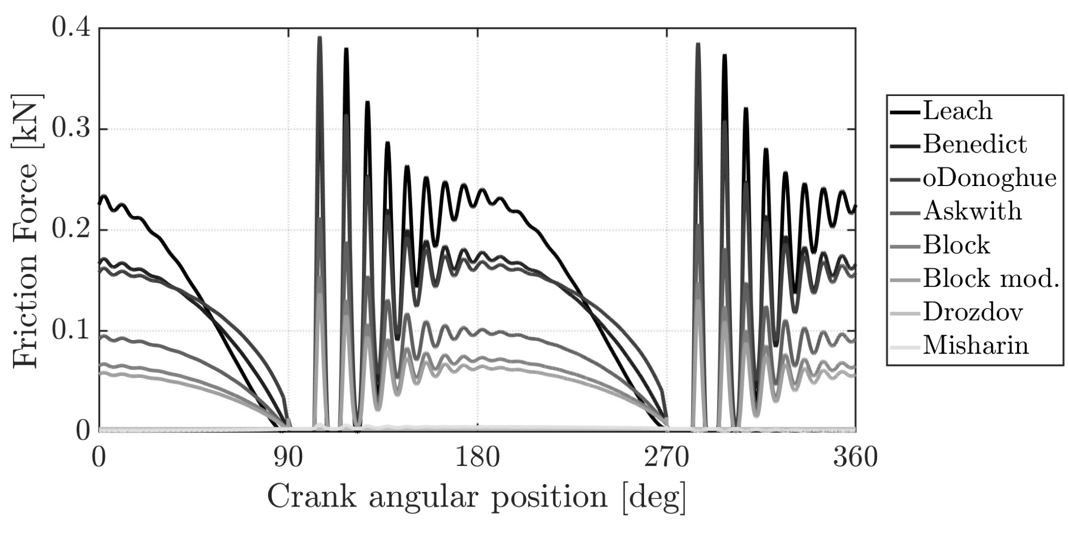

Figure 12: Friction force for different semi-empirical formulations.

happen only during the transition between the acceleration and deceleration phase of the slider, where a free-flight period of the pin and a change in the contact profile of the slot are observed. Conversely, the transition between the deceleration and acceleration phase occurs continuously, and no sudden variations

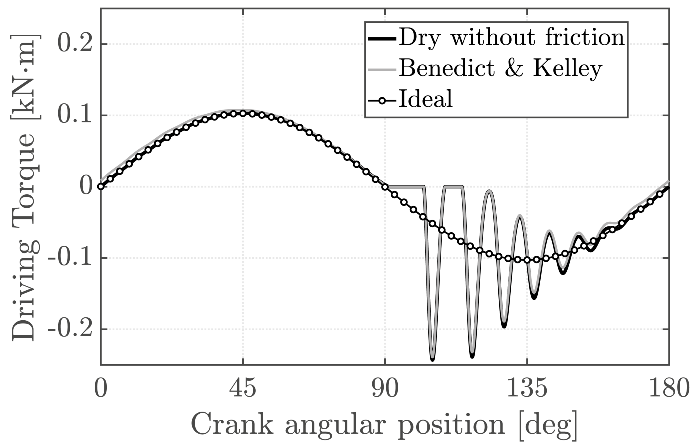

Figure 13: Comparison of driving torque between ideal and non-ideal cases.

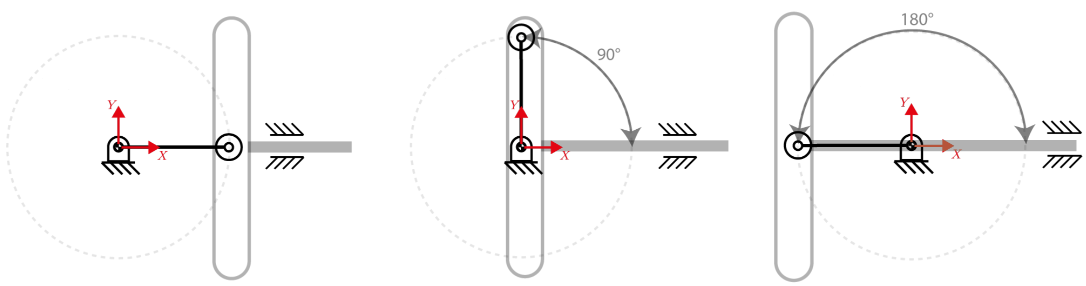

Figure 14: Mechanism configurations at 0, 90 and 180 degrees.

of the torque are observed. Having said that, and observing the mechanism configurations in Figure 14, for a constant crank speed, two phases can be observed in a crank rotation period of 180 degrees. In the first phase (*i.e.* between 0 and 90 degrees), the slider accelerates and therefore the driving torque is positive; the ideal case and the contact case without friction have little difference, while the driving torque slightly increases when friction is taken into account. In the second phase (*i.e.* between 90 and 180 degrees) the slider decelerates, so the driving torque is negative. In this case, the friction force tends to slow down the crank, helping the action of the motor. Because of this, the driving torque in the lubricated case is lower in absolute terms than in the dry one without friction. For any condition considered, the ratio between the computation time and the simulation time, using Matlab to perform the multibody simulation, is reported in Table 9. Even in the ideal case, a computation time 10 times longer than real time is obtained. This is due to the high rotation speed and low inertia of the system. Additionally, the ideal simulation was performed with the same integration tolerance as the contact cases for direct comparison of differences. A remarkable increase of run-time can be observed with the introduction of a non-ideal joint. In contrast, the introduction of friction models has not a relevant consequence on the run-time itself.

	Ideal joint	**Dry without friction**	**Dry with constant friction**
Ratio of computation time	10	89	89

	Lubricated models						
	Leach	Benedict	O'Donoguhue	Askwith	Block	Drozdov	Misharin
Ratio of computation time	104	104	112.5	108	106	100	98

Table 9: Ratio of computation time (average on 10 runs) to solve 4 full crank rotation for the Scotch-Yoke mechanism, with processor Intel I7-9750H, 2.60 GHz.

5.2 Case study 2: Whitworth quick return mechanism

In this second case study, dynamic simulations involved modeling the ideal system, the real system under dry contact conditions without friction, and the case with a constant friction coefficient $\mu = 0.1$. Subsequently, simulations were carried out for the lubricated case, considering variable friction coefficients based on the operational conditions described in Section 3.

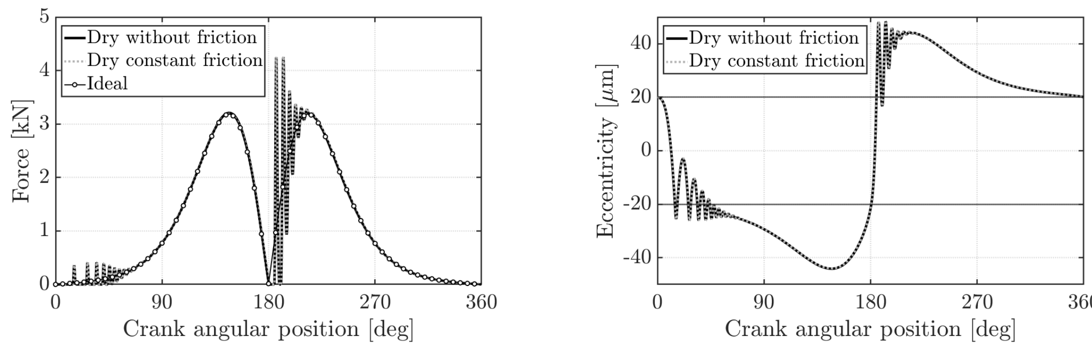

Figure 15: Normal contact force (left) and eccentricity of the pin (right) over a full cranckshaft revolution for the Whitworth quick return mechanism.

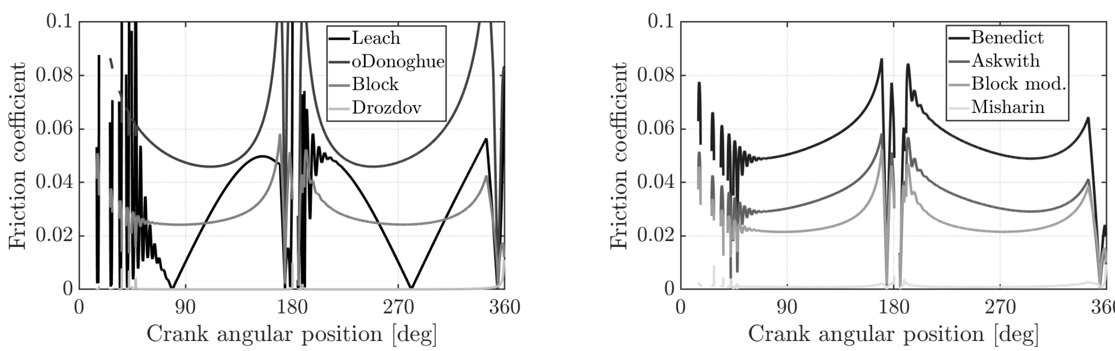

Figure 16: Friction coefficient according to different semi-empirical formulations applied to the Whitworth quick return mechanism.

In Figure 15, the left side illustrates the behavior of the normal contact force for the dry case, both without friction and with a constant friction coefficient, over a full crank revolution, compared to the reaction force of the prismatic joint in the ideal scenario. On the right side, the eccentricity of the pin is depicted, noting a clearance $c = 20$ μm in the slotted joint. Despite lower clearance and rotational speed compared to the previous case study, significant oscillations in the normal force occur due to high system accelerations around 180 degrees of crank rotation, corresponding to the quick return of the slider. However, the system does not exhibit chaotic dynamic behavior, thus remaining independent of initial conditions.

Regarding the case with mixed lubrication, Figure 16 illustrates the trends of the different formulations of the friction coefficient over one complete crank rotation. The simulations utilized the identical lubricant properties as in the previous case, outlined in Table 5.1. As a result, the average oil film thickness was determined to be $\overline{h_c} = 0.98\mu$m, which falls within the range defining the mixed lubrication regime. This slight increase from the previous case is attributed to the reduced contact forces experienced. First, it should be noted that, on average, lower friction coefficients values are obtained compared to the Scotch-Yoke mechanism. This is attributed to a slight decrease in normal load and a wider contact width, despite slightly lower sliding and rolling velocities due to the lower crank rotational speed. This is valid for all friction coefficients except for the O'Donoghue model, which shows higher values because it relies heavily on sliding velocity and is not influenced by the load. Indeed, a minimum can be observed corresponding to the crank angle at which the maximum sliding velocity occurs. Once again, the Leach model exhibits a different trend compared to the other models due to its strong dependency on the load. Additionally, there is a clear tendency towards a minimum value approaching zero at high sliding speeds and low normal force. Furthermore, Sasaki's formulation is unsuitable in this scenario as sliding velocities, though lower than the previous case, exceed the model's application bounds. Lemansky's formula is also inapplicable due to its dependence on the slot surface's curvature radius, which is infinite. Lastly, Drozdov and Misharin's models yield excessively low friction coefficient values due to high sliding velocities.

Figure 17, instead, compares the friction forces generated by the aforementioned friction coefficient models. As observed, the different friction coefficient trends result in rather similar tangential force trends, except for the absolute values associated with the mentioned average coefficients.

Finally, in Figure 18, the trend of the driving torque applied to the crankshaft is reported over one full revolution. This comparison includes the ideal case, the dry case without friction, and the lubricated case using the Benedict formula. In this scenario, it is apparent that the load cycle corresponds to a 360 degree period of the driving torque. In particular, four phases can be distinguished: The first phase spans from 0 to approximately 115 degrees, during which the system decelerates, the driving torque is negative and of minimal amplitude. This is attributed to the wide lever arm of the contact force in relation to the center of the slotted bar, resulting in a low normal contact force and negligible friction force. Consequently, no discernible difference is observed between the dry and lubricated cases. At around 115 degrees, the lever arm of the normal force relative to the center of the crankshaft becomes zero. The second phase, spanning from 110 to approximately 180 degrees, represents the acceleration period for the slotted bar and the slider.

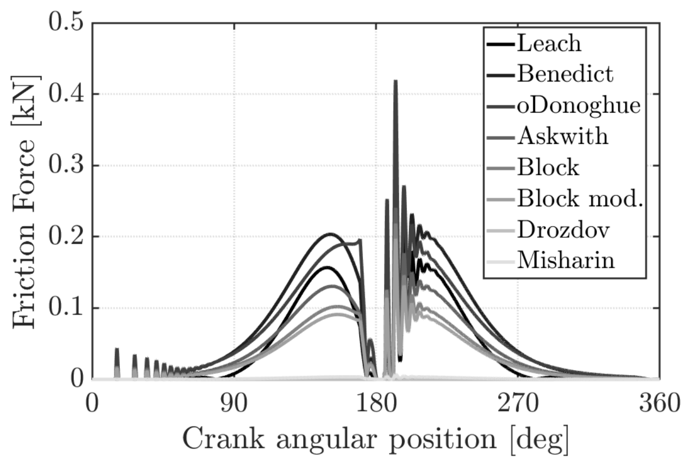

Figure 17: Friction forces according to different semi-empirical formulations applied to the Whitworth quick return mechanism.

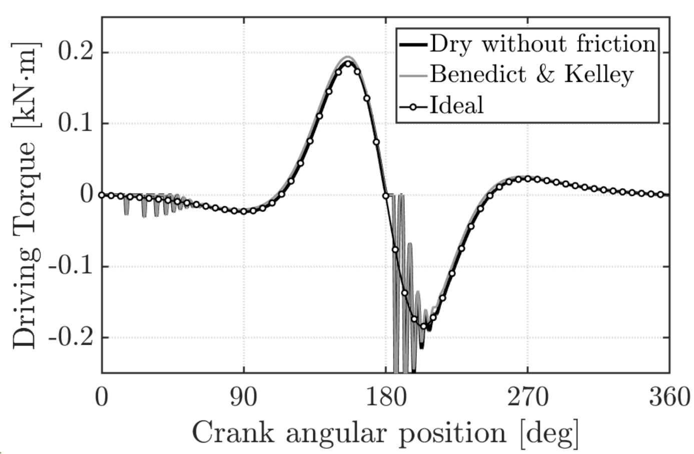

Figure 18: Comparison of driving torque between ideal and non-ideal cases for the Whitworth quick return mechanism.

During this phase, the driving torque is positive and the lever arm of the normal force relative to the center of the slotted bar decreases. The friction force is no longer negligible; indeed, an increase in torque is observed in the case with friction. A maximum point can be observed, corresponding to the maximum acceleration of the slotted bar and, consequently, the slider.During the third phase, spanning from 180 to 245 degrees, the system decelerates rapidly. The driving torque is negative and reaches a minimum corresponding to the maximum deceleration of the system. In conclusion, the fourth phase, extending from 245 to 360 degrees, denotes a phase of slight acceleration as the system returns to its initial configuration. In conclusion, during the fourth phase from 245 to 360 degrees, the system undergoes slight acceleration, returning to its initial state while experiencing an increase in the lever arm of the normal force relative to the center of the slotted bar.

In Table 10 the ratio between computation time and simulation time is reported for this mechanism. Compared to the previous case, computation times are reduced due to lower crankshaft rotation speed and increased body inertia. Similarly to the previous case, instead, the introduction of friction formulation results in a slight increase in computation times compared to the dry case without friction.

	Ideal joint	**Dry without friction**	**Dry with constant friction**
Ratio of computation time	1.5	15	16

	Lubricated models						
	Leach	Benedict	O'Donoguhue	Askwith	Block	Drozdov	Misharin
Ratio of computation time	18	17.5	18	17.5	18	18	17

Table 10: Ratio of computation time (average on 10 runs) to solve 4 full crank rotation for the Whitworth quick return mechanism, with processor Intel I7-9750H, 2.60 GHz

6 Conclusions

In this work, semi-empirical tools for embedding friction into non stationary mechanical systems with unilateral contacts under sliding and rolling conditions have been suggested. These formulations are derived for the contact between gear teeth and are generally valid models for conditions similar to those, i.e., where an elastohydrodynamic lubrication regime is present. Initially, a review of the different formulations developed in the literature was conducted, and trends of friction coefficients were plotted as a function of sliding velocity and normal load on the contacting surfaces, highlighting their main characteristics and differences among various formulations. Subsequently, these formulations are applied within multibody simulations where non-ideal kinematic pairs with clearance are present, and their applicability for calculating the friction force is demonstrated. A scotch-yoke mechanism and a Whitworth quick return mechanism are chosen as the linkages to be tested, in which the contact between the pin and the slot is counterformal, typically resulting in a regime of total or partial elastohydrodynamic lubrication. Due to such lubrication condition, the contact stiffness is minimally influenced by the oil film. Therefore, for the evaluation of the normal contact force, the Lankarani-Nikravesh model was used, adjusting the stiffness coefficient and the non-linearity exponent for the case of cylindrical contact. Meanwhile, for the friction force model, a modified Coulombian model was used, which does not account for the stiction phenomenon. From the results, it can be concluded that the Benedict & Kelley, Askwith *et al.* and Block models are consistent and show comparable trends. While the formulation proposed by O'Donoghue & Cameron exhibits a friction coefficient trend similar to the previous ones in the case of the Scotch Yoke, it differs in its application to the Whitworth mechanism due to lower sliding velocities. Conversely, the Leach & Kelley model exhibits a significant dependence on the load. Lastly, the Drozdov and Misharin models return very low friction coefficients for high sliding velocities. The Sasaki formulation, on the other hand, is not applicable for high sliding velocities unless the normal load exceeds a certain threshold. Instead, Lemansky's formulation is not valid for cases where the slot is flat, as the formula explicitly includes the radius of curvature of the surfaces. Using these models in multibody simulations, the computational cost does not significantly increase compared to imposing a constant friction coefficient. Another advantage of these models is that the system exhibits a non-stiff behavior, unlike hydrodynamic models where adjusting simulation parameters is necessary to avoid numerical errors. In conclusion, it has been demonstrated how such friction coefficient models can be incorporated into multibody dynamic simulations, allowing for the variability of these coefficients under operational conditions. The choice of the correct coefficient depends on the specific case and should be supported by experimental data. However, in addition to compiling the semi-empirical formulations developed by researchers, the article enhances understanding of the distinctions among the different models and could potentially provide guidance for selecting the suitable friction formulation, depending upon the specific application requirements. Finally, the analytical comparisons performed here and all the observations reported are specific to the situations under study and may not apply to other situations.

Acknowledgement

This research was funded by Italian Ministry for University and Research, project PRIN 2020: "Innovative Contact Based multibody models for noise and vibration prediction in high-performance gears" grant number 202022Y4N5.

References

[1] Coulomb, C.A.: Théorie des machines simples, en ayant égard au frottement de leurs parties, et à la roideur des cordages. Bachelier (1809)

[2] Morin, A.: Note sur la resistance au roulement des corps les uns sur les autres et sur le reaction elastique des corps qui se comprime reciproquement. Comptes rendus de l'Académie des Sciences **13** (1841) 1022–1023

[3] Reynolds, O.: On rolling-friction. Philosophical Transactions of the Royal Society of London **166** (dec 1876) 155–174

[4] Merritt, H.E.: Worm gear performance. Proceedings of the Institution of Mechanical Engineers **129**(1) (jun 1935) 127–194

[5] Tabor, D.: The mechanism of rolling friction II. the elastic range. Proceedings of the Royal Society of London. Series A. Mathematical and Physical Sciences **229**(1177) (apr 1955) 198–220

[6] Eldredge, K., Tabor, D.: The mechanism of rolling friction. i. the plastic range. Proceedings of the Royal Society of London. Series A. Mathematical and Physical Sciences **229**(1177) (apr 1955) 181–198

[7] Bowden, F.P., Tabor, D.: Friction, lubrication and wear: a survey of work during the last decade. British Journal of Applied Physics **17**(12) (dec 1966) 1521–1544

[8] Hersey, M.D.: Rolling friction, I - Historical introduction. Journal of Lubrication Technology **91**(2) (apr 1969) 260–263

[9] Hersey, M.D.: Rolling friction, III - Review of later investigations. Journal of Lubrication Technology **91**(2) (apr 1969) 269–275

[10] Martin, K.: A review of friction predictions in gear teeth. Wear : an international journal on the science and technology of friction lubrication and wear **49**(2) (aug 1978) 201–238

[11] Michlin, Y., Myunster, V.: Determination of power losses in gear transmissions with rolling and sliding friction incorporated. Mechanism and Machine Theory **37**(2) (feb 2002) 167–174

[12] Stefanelli, R., Valentini, P.P., Vita, L.: Modelling hydrodynamic journal bearing in 3d multibody systems. In: ASME-IDETC/CIE 2005, Long Beach, California, USA, American Society of Mechanical Engineers (sep 2005)

[13] Flores, P., Ambrósio, J.A.C.: Revolute joints with clearance in multibody systems. Computers & structures **82**(17-19) (jul 2004) 1359–1369

[14] Flores, P., Ambrósio, J.A.C., Pimenta Claro, J.C., Lankarani, H.M., Koshy, C.S.: A study on dynamics of mechanical systems including joints with clearance and lubrication. Mechanism and Machine Theory **41**(3) (mar 2006) 247–261

[15] Zhao, B., Cui, Y., Xie, Y., Zhou, K.: Dynamics and lubrication analyses of a planar multibody system with multiple lubricated joints. Proceedings of the Institution of Mechanical Engineers, Part J: Journal of Engineering Tribology **232**(3) (2018) 326–346

[16] Zhao, B., Zhou, K., Xie, Y.: A new numerical method for planar multibody system with mixed lubricated revolute joint. International Journal of Mechanical Sciences **113** (2016) 105–119

[17] Fang, C., Meng, X., Lu, Z., Wu, G., Tang, D., Zhao, B.: Modeling a lubricated full-floating pin bearing in planar multibody systems. Tribology International **131** (2019) 222–237

[18] Velex, P., Cahouet, V.: Experimental and numerical investigations on the influence of tooth friction in spur and helical gear dynamics. J. Mech. Des. **122**(4) (2000) 515–522

[19] Mushirabwoba, B., Belfals, L., Brahim, N., Abdelilah, L.: A comparative study of friction laws used in spur gear power losses estimation. Contemporary Engineering Sciences **9**(6) (2016) 279–288

[20] Song, N., Peng, H., Kan, Z., Chen, B.: A novel nonsmooth approach for flexible multibody systems with contact and friction in 3D space. Nonlinear Dynamics **102**(3) (November 2020) 1375–1408

[21] Peng, H., Song, N., Li, F., Tang, S.: A Mechanistic-Based Data-Driven Approach for General Friction Modeling in Complex Mechanical System. Journal of Applied Mechanics **89**(7) (05 2022) 071005

[22] Kan, Z., Peng, H., Chen, B.: A simple linear complementarity approach for sliding cable modeling considering friction. Mechanical Systems and Signal Processing **130** (2019) 293–314

[23] Song, N., Zhang, M., Li, F., Kan, Z., Zhao, J., Peng, H.: Dynamic research on winding and capturing of tensegrity flexible manipulator. Mechanism and Machine Theory **193** (2024) 105554

[24] Flores, P., Ambrósio, J.A.C., Pimenta Claro, J.C., Lankarani, H.M.: Kinematics and Dynamics of Multibody Systems with Imperfect Joints: Models and Case Studies. Springer International Publishing (2010)

[25] Flores, P., Lankarani, H.M.: Contact force models for multibody dynamics. Volume 226 of Solid mechanics and its applications. Springer International Publishing, Cham (2016)

[26] Autiero, M., Cera, M., Cirelli, M., Pennestrì, E., Valentini, P.P.: Review with analytical-numerical comparison of contact force models for slotted joints in machines. Machines **10**(11) (2022) 966

[27] Schwab, A., Meijaard, J., Meijers, P.: A comparison of revolute joint clearance models in the dynamic analysis of rigid and elastic mechanical systems. Mechanism and Machine Theory **37**(9) (sep 2002) 895–913

[28] Pereira, C., Ramalho, A., Ambrósio, J.A.C.: Experimental and numerical validation of an enhanced cylindrical contact force model. In De Hosson, J.M., Brebbia, C., eds.: Surface Effects and Contact Mechanics X. Volume 1 of WIT transactions on engineering sciences., Southampton, UK, WIT Press (sep 2011) 49–60

[29] Pereira, C., Ramalho, A., Ambrósio, J.A.C.: Applicability domain of internal cylindrical contact force models. Mechanism and Machine Theory **78** (aug 2014) 141–157

[30] Skrinjar, L., Slavič, J., Boltežar, M.: A validated model for a pin-slot clearance joint. Nonlinear Dynamics **88**(1) (apr 2017) 131–143

[31] Skrinjar, L., Slavič, J., Boltežar, M.: A review of continuous contact-force models in multibody dynamics. International Journal of Mechanical Sciences **145** (sep 2018) 171–187

[32] Lankarani, H.M., Nikravesh, P.E.: A contact force model with hysteresis damping for impact analysis of multibody systems. Journal of Mechanical Design **112**(3) (sep 1990) 369–376

[33] Pereira, C., Ramalho, A., Ambrosio, J.: An enhanced cylindrical contact force model. Multibody System Dynamics **35** (2015) 277–298

[34] Johnson, K.L.: Contact Mechanics. Reprint edn. Cambridge University Press (2008)

[35] Pennestrì, E., Rossi, V., Salvini, P., Valentini, P.P.: Review and comparison of dry friction force models. Nonlinear dynamics **83** (2016) 1785–1801

[36] Andersson, S., Söderberg, A., Björklund, S.: Friction models for sliding dry, boundary and mixed lubricated contacts. Tribology international **40**(4) (2007) 580–587

[37] Zhang, Y., Liu, H., Zhu, C., Liu, M., Song, C.: Oil film stiffness and damping in an elastohydrodynamic lubrication line contact-vibration. Journal of Mechanical Science and Technology **30** (2016) 3031–3039

[38] Stribeck, R.: Die wesentlichen eigenschaften der gleit-und rollenlager. Zeitschrift des Vereines Deutscher Ingenieure **46** (1902) 1341–1348

[39] Benedict, G.H., Kelley, B.W.: Instantaneous coefficients of gear tooth friction. A S L E Transactions **4**(1) (jan 1961) 59–70

[40] Tallián, T.: The theory of partial elastohydrodynamic contacts. Wear **21** (1972) 49–101

[41] Arana, A., Larrañaga, J., Ulacia, I.: Partial ehl friction coefficient model to predict power losses in cylindrical gears. Proceedings of the Institution of Mechanical Engineers, Part J: Journal of Engineering Tribology **233**(2) (2019) 303–316

[42] Xu, H.: A novel formula for instantaneous coefficients of sliding friction in gearing. Technical report, SAE Technical Paper (2007)

[43] Autiero, M., Cirelli, M., Paoli, G., Valentini, P.P.: A data-driven approach to estimate the power loss and thermal behaviour of cylindrical gearboxes under transient operating conditions. Lubricants **11**(7) (2023) 303

[44] Anderson, N.E., Loewenthal, S.H.: Design of spur gears for improved efficiency. (1982)

[45] Blok, H.: Hydrodynamic effects on friction in rolling with slippage. In Bidwell, J., ed.: Rolling contact phenomena, Elsevier Publishing Company (1962) 186–251

[46] Misharin, Y.: Influence of the friction conditions on the magnitude of the friction cefficients in the case of rolling with sliding. In: Proceedings International Conference on Gearing, Institution of Mechanical Engineers (1958) 159–164

[47] Sasaki, T., Okamura, K., Isogai, R.: Fundamental research on gear lubrication. Bulletin of JSME **4**(14) (1961) 382–394

[48] Askwith, T., Crouch, R., Cameron, A.: The relationship of lubricants and additives for optimum effect; and a theory of scuffing. In: Proceedings International Conference on Gear Lubrication, Institution of Mechanical Engineers (1966)

[49] Kelley, B.W., Lemanski, A.J.: Paper 11: lubrication of involute gearing. Proceedings of the Institution of Mechanical Engineers, Conference Proceedings **182**(1) (sep 1967) 173–184

[50] Leach, E.F., Kelley, B.W.: Temperature - The key to lubricant capacity. A S L E Transactions **8**(3) (jan 1965) 271–285

[51] O'Donoghue, J.P., Cameron, A.: Friction and temperature in rolling sliding contacts. A S L E Transactions **9**(2) (jan 1966) 186–194

[52] Drozdov, Y., Gavrikov, Y.: Friction and scoring under the conditions of simultaneous rolling and sliding of bodies. Wear : an international journal on the science and technology of friction lubrication and wear **11**(4) (apr 1968) 291–302

[53] Baumgarte, J.: Stabilization of constraints and integrals of motion in dynamical systems. Computer Methods in Applied Mechanics and Engineering **1**(1) (1972) 1–16

[54] Hamrock, B.J., Dowson, D.: Isothermal elastohydrodynamic lubrication of point contacts: part iii—fully flooded results. (1977)